Energy 294 (2024) 130765

Contents lists available at ScienceDirect

Energy

journal homepage: www.elsevier.com/locate/energy

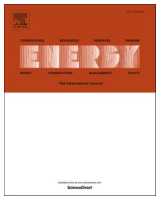

Optimal energy management system for grid-connected hybrid power plant and battery integrated into multilevel configuration

Ehsan Hosseini [a], Pablo Horrillo-Quintero [a], David Carrasco-Gonzalez [a], Pablo García-Triviño [a], Raúl Sarrias-Mena [b], Carlos A. García-Vázquez [a], Luis M. Fernández-Ramírez [a,*]

[a] Research Group in Sustainable and Renewable Electrical Technologies (PAIDI-TEP023), Department of Electrical Engineering, Higher Technical School of Engineering of Algeciras (ETSIA), University of Cádiz, Avda. Ramón Puyol, s/n. 11202 Algeciras, Cádiz, Spain

[b] Research Group in Sustainable and Renewable Electrical Technologies (PAIDI-TEP023), Department of Engineering in Automation, Electronics and Computer Architecture & Networks, Higher Technical School of Engineering of Algeciras (ETSIA), University of Cádiz, Avda. Ramón Puyol, s/n. 11202 Algeciras, Cádiz, Spain

ARTICLE INFO

Handling editor: A Mellit

Keywords:
Energy storage system
Optimal energy management
Multi-level inverter
Wind turbine
Photovoltaic cells

ABSTRACT

A novel optimal energy management system (EMS) using a nonlinear constrained multivariable function to optimize the operation of battery energy storages (BESs) used in a hybrid power plant with wind turbine (WT) and photovoltaic (PV) power plants is proposed in this work. The hybrid power plant uses a configuration based on a battery-stored impedance-based cascaded multilevel inverter to integrate renewable energy sources (PV power plants and WT) and BESs into the grid. The new optimal EMS seeks for satisfying the demanded power while dispatching power between BESs to optimize their efficiency. A grid-connected configuration is implemented to assess the efficiency of the suggested supervisory control under changes in renewable energy (changes in wind speed and irradiation), and in a varying active and reactive powers' request. The BES efficiency obtained from the suggested EMS is set side by side to the BES efficiency got from a conventional EMS and a model predictive control (MPC), both working based on the state-of-charge (SOC) of the BES and balancing power EMS. The results from MATLAB simulation and the experimental results with the real-time OPAL-RT simulator (OP4510, OPAL-RT) and dSPACE MicroLabBox show the effectiveness of the suggested approach and the improvement in long-term BES efficiency.

1. Introduction

Sustainable and environmentally friendly renewable energy sources (RESs) and energy savings are gaining more penetration in power systems as clean alternatives [1]. Currently, wind turbine (WT) and photovoltaic (PV) plants are considered as the most favourable RESs, because they provide a large endless amount of clean energy. However, the intermittent characteristics of these sources and their dependency on environmental conditions negatively affect consumer needs [2]. Therefore, to counterbalance the stochastic nature of PV and WT energy sources, energy stored systems (ESS) are being applied, and in the other words, to compensate for the power demand that RES cannot satisfy or to store power not requested [3]. Electrochemical batteries are typically used as ESS because of their low cost and non-toxicity in term of batteries recycling [4].

However, the energy produced by the RESs always fluctuates, and converting it to an appropriate AC voltage and frequency power is crucial. The interface between the sources and stand-alone load or grid is fulfilled by using power converters to transfer reliable and efficient energy to the consumer side. Voltage-source converter (VSC) by two-level has been applied for energy conversion in industry, however its usage is limited in high power and switching ranges due to semiconductor manufacturing technology of silicon carbide or gallium nitride [5,6]. Hence, multilevel converters and connected switch cells have been introduced for applications in high-power systems to take advantage of the synthesized output voltage level and improve harmonic performance. In Ref. [7], series/parallel-connected switch cells were proposed for high-voltage high-power converters. However, because of various practical limitations, the series-connected switch cell's number is restricted, and they cannot be constructed for any voltage level.

* Corresponding author.
E-mail addresses: ehsan.hosseini@uca.es (E. Hosseini), pablo.horrillo@uca.es (P. Horrillo-Quintero), david.carrasco@uca.es (D. Carrasco-Gonzalez), pablo.garcia@uca.es (P. García-Triviño), raul.sarrias@uca.es (R. Sarrias-Mena), carlosandres.garcia@uca.es (C.A. García-Vázquez), luis.fernandez@uca.es (L.M. Fernández-Ramírez).

https://doi.org/10.1016/j.energy.2024.130765
Received 26 July 2023; Received in revised form 29 January 2024; Accepted 20 February 2024
Available online 21 February 2024

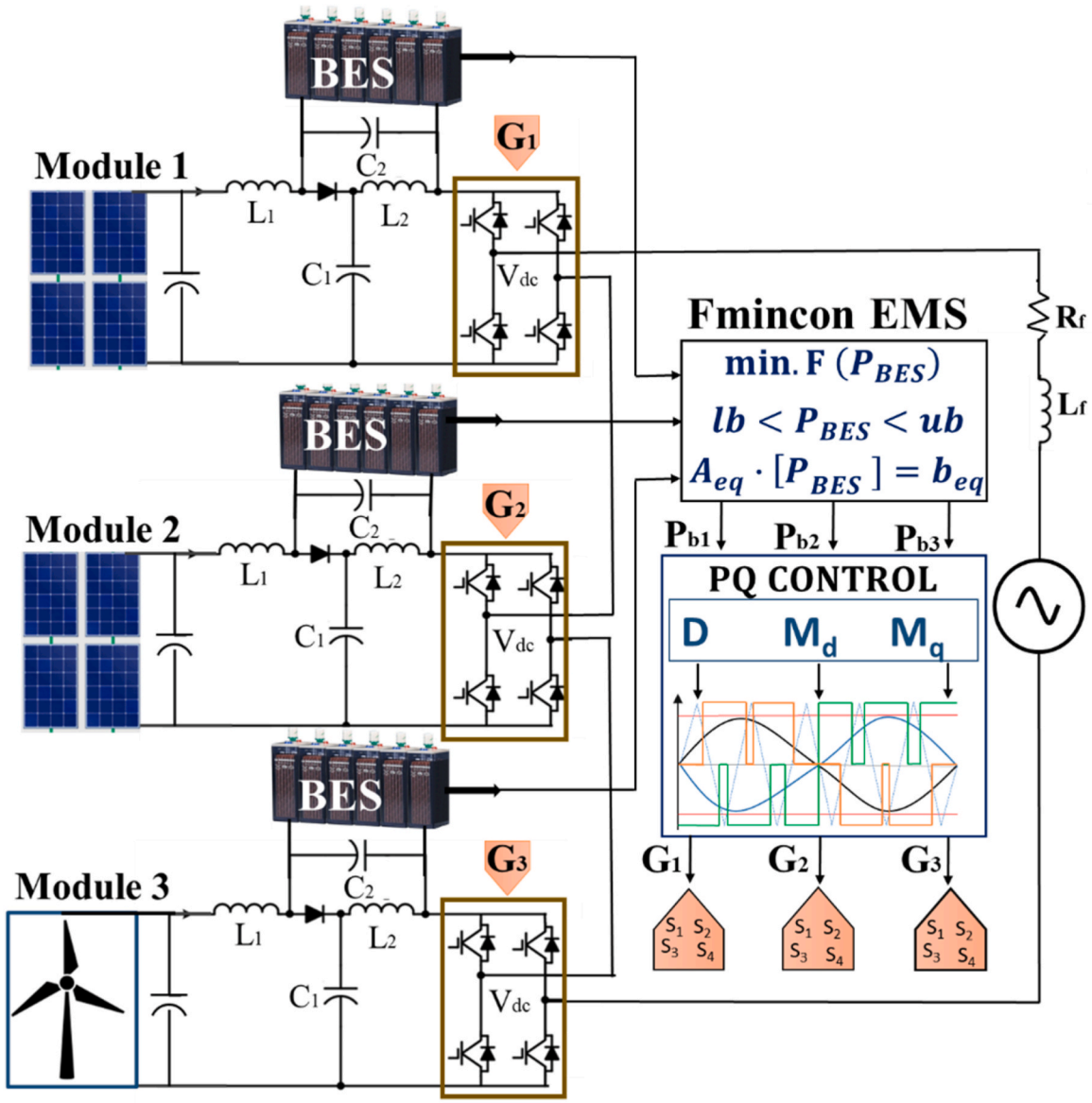

Fig. 1. Hybrid power plant under study based on BES-qZS-CHBMLI and RES (PV power plants and WT) and control system.

Multilevel configurations have been introduced as another option to meet the voltage requirements of high-power systems [8]. One proposed multilevel configuration is a cascaded H-bridge multilevel VSC configured by multiple single-phase H/full-bridges connection in series. The necessity of multiple isolated DC sources in each module makes this topology expensive (if RES is not used), whereas it is attractive for reactive power exchange, as in static synchronous compensator (STATCOM) applications. Furthermore, to achieve the desired voltage level, corresponding open-winding transformers are used in the AC-side connection. Another class of multilevel converters is the flying-capacitor multilevel VSC configuration [9]. Many relatively large capacitors are used; therefore, the regulation of capacitor voltages is challenging. To avoid the drawbacks of the aforementioned multilevel converter class, a diode-clamped multilevel VSC was realized at different voltage levels [10]. Although this converter offers lower switching losses and stress and a less distorted synthesized AC voltage, it requires a multimodule structure for high-voltage applications.

Conventional multilevel inverter/converters and impedance-based sources, also called Z-source inverters (ZSIs), have received considerable attention because they provide interesting characteristics that fit them for RES applications combined with ESS [11]. Offering a shoot-through (ST) state during the zero-state interval enables this inverter type boosting the input voltage, which in turn expands inverter application fields and improves its reliability. To improve some characteristics of the typical impedance inverter, quasi-ZSI (qZSI) has been suggested as a topology modification that can be used for energy conversion purposes in multilevel cascaded structures [12]. Several qZSIs can be prepared to provide a cascaded H-bridge multilevel inverter (CHBMLI) structure and can be easily scaled by increasing the modules while there is no need to add a voltage transformer like conventional structures at the inverter output. In this case, the values of output filter components are smaller than those of the other multilevel configurations [13].

qZS-CHBMLIs were applied to PV power plants in Refs. [14–16]. qZS-CHBMLI, which integrates an ESS, mainly a BES (BES-qZS-CHBMLI), is an interesting option for PV power plants to compensate the lack of energy during the night and save the extra energy during the day. Integration of ESS into the impedance network of a qZS-CHBMLI eliminates the need for a DC-DC converter to connect and operate the ESS [17], allowing the support of the PV power plant.

Using ESS to back up renewable energy sources or saving produced energy requires a suitable EMS is essential for creating a reliable,

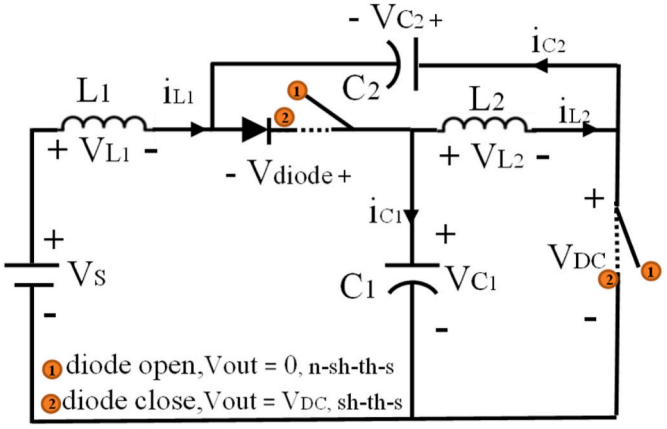

Fig. 2. Shoot-through and non-shoot-through equivalent circuits states.

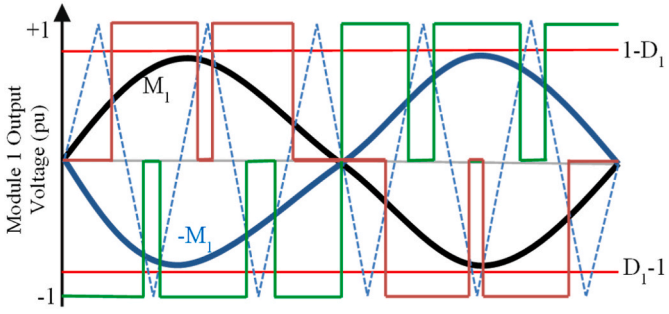

Fig. 3. Modulation scheme used for each BES-qZSI module.

sustainable, and well-operating energy [18,17]. In Ref. [19] an algorithm is tailored for managing energy in a specific system architecture (BES-qZS-CHBMLI with PV systems) over a 24-h period. Its key feature is the utilization of the SOC of each BES for optimizing the distribution of power to cover the difference between energy generation and consumption. The EMSs were utilized consistently in Refs. [20,21] for the integration of PV systems and BES within a BES-qZS-CHBMLI architecture. The focus is on maintaining balance among the SOCs of different modules, irrespective of variations in solar irradiance.

Another EMS based on distributing power depending on BES SOC was suggested in Ref. [22] for a BES-qZS-CHBMLI with PV systems, limiting the SOCs between the minimum and maximum safety values and dispatching the maximum charge or discharge power to its nominal power. In Ref. [23], a model predictive control (MPC)-based EMS was designed to a BES-qZS-CHBMLI with PV systems. The proposed EMS, where less computational effort was needed in the design of the MPC, diminishes the double line BES current frequency ripple. In this study, among the total number of submodules the total active power reference was divided with the same amount; however, for real systems, each module supplied by the RES can operate with a different output power.

Regarding the system topology, few studies have addressed the dynamics of grid-connected AC MGs with hybrid power plants, BESs and an optimized EMS. Previous works have primarily employed a configuration based on DC/DC converter and VSI [24], while this study proposes a topology based on ES-qZS-CHBMLI without an additional DC/DC converter. Moreover, previous studies with power plants based on BES-qZS-CHBMLI have used a uniform configuration, incorporating the same PV systems and BESs into each module in series, while this work explores the integration of PV or WT and BES with different nominal powers in each module. Additionally, the evaluation of grid performance in terms of active and reactive powers demands has often been overlooked.

Regarding the EMS, previous works have focused on distributing the power among the BESs based on to their SOC, neglecting the efficiency of BESs. This study proposes an EMS that considers both SOC and BES efficiency to optimize power distribution.

To cover the gaps mentioned in previous studies, the key aspects of the approach and contributions of this paper are: 1) Integration of hybrid RES and different BESs into a hybrid power plant: Unlike previous studies, this work proposes a hybrid power plant based on a BES-qZS-CHBMIL comprising hybrid RES (WT and PV systems, and not only PV power plants), and different BESs (and not the same BESs) within each module connected in series, while also accommodating operator power requests within the controller design. 2) Development of an optimal EMS for efficient power dispatch and BES management: A novel EMS is developed to optimize power dispatch among the BESs to maximize efficiency while ensuring compliance with BES charging/discharging limitations, while meeting the power demand. This optimization approach aims to extend battery lifespan and reduce degradation. The EMS considers both nominal battery parameters and real-time values. The proposed EMS is based on optimizing the global BES efficiency by using a nonlinear objective function. In this EMS, an optimization algorithm based on a MATLAB function called fmincon is applied to solve the optimization problem and determine how the BES must operate, together with the PV cells and WT, to meet the power requirements (active and reactive powers) requested by the grid operator, and simultaneously, to maximize the global efficiency of BESs integrated into the hybrid power system. The posed EMS designed for a hybrid system is assessed under variable wind speed and solar irradiation, and active and reactive power references defined by the system operator, and the results are compared with those obtained from the conventional EMS based on the SOC and MPC methods. 3) The performance of the hybrid power plant, control system, and EMS is comprehensively evaluated through experimental testing based on hardware-in-the-loop (HIL) setup.

The structure of this paper is as follows. Section 2 presents the system under study based on BES-qZS-CHBMLIs with PV power plants and WT. Section 3 illustrates the implemented system control and proposed optimal EMS. Section 4 presents and discusses the simulation results and Section V shows the experimental real-time results. At the end, the conclusions are provided in Section 5.

2. System under study

The hybrid power plant under study is composed of three BES-qZSI series-connected modules (BES-qZS-CHBMLI) to a single-phase grid. The first two BES-qZSI modules are fed by independent PV power plants and the third module is fed by a WT. In each module, a different BES is considered as parallel-connected in capacitor C_2 of the impedance network to support and store the renewable energy generated from the PV power plant or WT connected to the input of each module. Fig. 1 illustrates the hybrid power plant under study and the control system. The independent MPPT control for the PV power plants and WT is also included in the control design and is discussed in the next section.

Each module uses a qZSI, which is composed of H-bridge IGBT switches and a Z-network with two capacitors (C_1 and C_2) and two inductors (L_1 and L_2).

qZSI presents two states: non-shoot-through states and shoot-through [11]. During the non-shoot-trough state, the qZSI provides six active and two zero states of a conventional inverter, and thus, the diode conducts and the RES and inductors of the qZSI charge the capacitors and feed the inverter. In the shoot-through state, the two switches of one arm are closed at the same time, and thus, the diode is cut off so that the inductors of qZSI are charged by the RES and capacitors, and the inverter DC voltage is zero. Fig. 2 shows the equivalent circuit for both states. In each module, the inverter DC voltage (V_{DC}) can be calculated as the sum of the voltages across capacitors C_1 and C_2.

V_{DC} is expressed as a function of the shoot-through duty cycle (D) and the input voltage of qZSI (V_{in}) [11]:

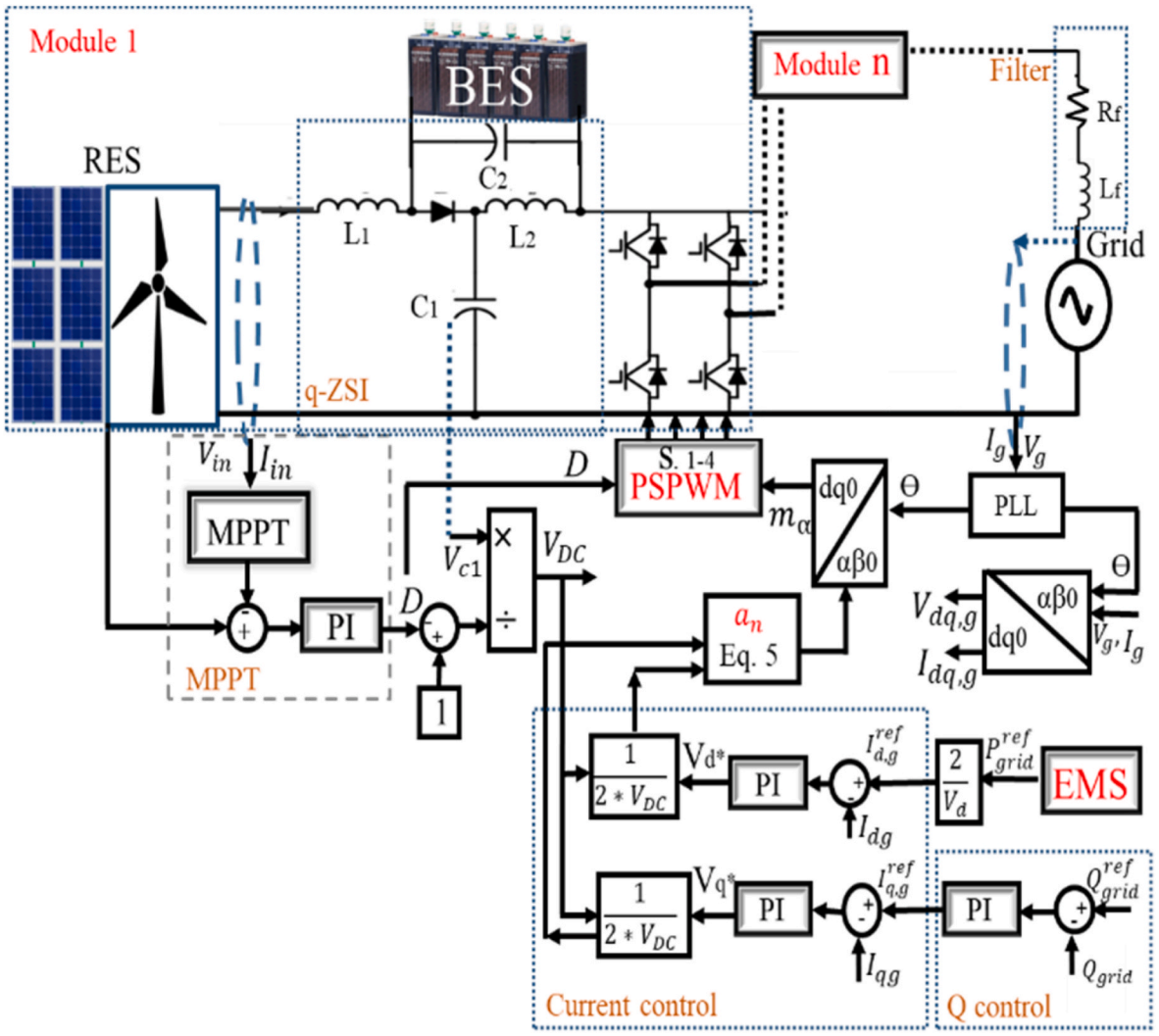

Fig. 4. Control scheme of each qZSI module.

$$V_{DC} = V_{C1} + V_{C2} = \frac{1}{1-2D} V_{in} \quad (1)$$

To transfer the energy available in the RES and BES to the grid, the switches of the VSI are controlled using phase-shift pulse-width modulation (PS-PWM) [25]. As shown in Fig. 3, this modulation method uses for each BES-qZSI module (i-module): 1) two signals dependent on the shoot-through duty cycle D_i ($1 - D_i$ and $D_i - 1$), which is obtained from the MPPT control of the RES (Section 3.1); a) two signals dependent on the modulation index M_i (M_i and $-M_i$), which is found by the grid power control (Section 3.2); and b) the carrier signal, which is shifted $180^\circ / n$ for each module, where n is the number of series-modules ($n = 3$, in this work).

3. Control system

This section illustrates the control systems used for the MPPT of the RES, and for the injected power to the grid, which are based on adjusting the modulation index (M_i) of each qZSI, and the shoot-through duty ratio (D_i), and the optimal EMS for the hybrid plant.

3.1. MPPT for PV power plants and WT

To find the DC voltage of the RES (PV power plant or WT) connected at the input of the qZSI, Perturb and Observe (P&O) method is applied, which allows MPPT to be achieved depending on the temperature and radiation of the PV cells and the wind speed of the WT. In each qZSI, D_i is used to control and boost the DC voltage. The independent MPPT control for the PV power plants and the WT is illustrated in Fig. 4.

The DC voltage and current measured for each renewable energy source are used in the MPPT controller to determine the reference DC voltage. A PI controller tunes D_i to track the reference DC link voltage to achieve the RES to operate at MPPT.

3.2. Grid reactive and active power control

To control the injecting reactive power (Q) and active power (P) to the grid, first the phase angle of the grid current and voltage are obtained from a phase locked loop (PLL). The control of P and Q is implemented through separate control loops at a d-q synchronous reference frame, where the d-component is used to control P and q-component to control Q. In single-phase systems [20], the voltage and current variables are converted to the α-β frame, where the β imaginary signal is equal to the real component α but delayed by a ¼ period. The orthogonal α-β frame are then changed into a rotation coordinate frame d-q.

Two separate d-q control loops are used to control P and Q delivered to the grid using the modulation index M, as shown in Fig. 4.

To control P, a control loop for the d-component current (i_d) is implemented in each qZSI. The overall delivered active power toward the grid is the sum power of the RES, including the two PV power plants,

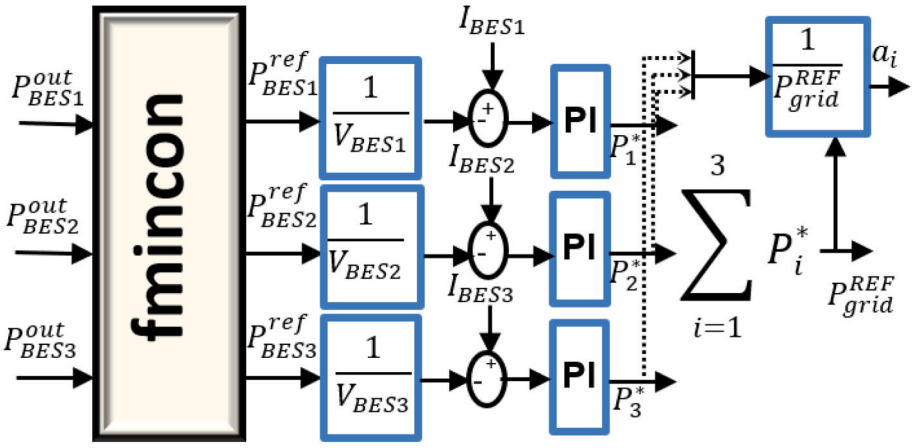

Fig. 5. Control scheme implemented in the EMS.

WT, and BES. Therefore, the total power reference (P_{grid}^{ref}) is defined by summing of the power reference for the qZSIs (P_i^*) as:

$$P_{grid}^{ref} = \sum_{i=1}^{3} P_i^* \tag{2}$$

where i is the module's number, and P_i^* is calculated by the EMS which will be discussed below.

The grid current peak (i_{grid}^*) is found by the grid voltage (V_{grid}) and the power reference for each qZSI [22]:

$$i_{grid}^* = \frac{2 \bullet \sum_{i=1}^{3} P_i^*}{V_{grid}} \tag{3}$$

The controlled d-component of the grid voltage (V_d) is used to calculate the d-component of the modulation index M_i ($m_{d,i}$) of each module. This $m_{d,i}$ is inserted into the phase-shifted-PWM (PS-PWM) method to be compared with carrier signal.

$$m_{d,i} = \frac{2 \bullet a_i \bullet V_d}{V_{pn,i}} \tag{4}$$

where a_i refers to the power factor of each module, defined as the relationship between the power reference for each qZSI and the total power reference, which can be calculated as follows.

$$a_i = \frac{P_i^*}{P_{grid}^{ref}} \tag{5}$$

To control Q, a control loop for the q-component current (i_q) is implemented in each qZSI (similar to the P control scheme) using the q-frame of M_i ($m_{q,i}$).

Once $m_{d,i}, m_{q,i}$ are obtained from the control loops of P and Q, the α-component of the modulation index ($m_{\alpha,i}$) is calculated. At the end, the IGBTs commands are generated from $m_{\alpha,i}$ and D_i according to the modulation scheme shown in Fig. 3.

3.3. Optimal EMS

The EMS posed here is responsible to set the BES reference power of the inserted BES to the ES-qZS-CHBMLI to optimize the BES efficiency while satisfying the system power balance and providing the demanded grid active and reactive powers. Fig. 5 illustrates the control scheme implemented in the EMS.

In the EMS, an objective function placed on optimizing the global BES efficiency of the hybrid power plant is implemented (Eq. (6)), and a constrained nonlinear multivariable algorithm, fmincon MATLAB function, is applied to determine the optimal solutions. The constraints defined for fmincon function are based on limiting the maximum power capacity of BESs, maintaining the SOC values, and covering the gap between the produced power and the requested one. The global BES efficiency to be maximized (η_{BES}) is calculated from Eq. (7) by:

$$min\ \{OF = 1 - \eta_{BES}\} \tag{6}$$

$$\eta_{BES} = \frac{P_{BES,1} + P_{BES,2} + P_{BES,3}}{P_{BES,1}^{in} + P_{BES,2}^{in} + P_{BES,3}^{in}} = \frac{P_{BES,1} + P_{BES,2} + P_{BES,3}}{\left(P_{BES,1}/\eta_{BES,1}\right) + \left(P_{BES,2}/\eta_{BES,2}\right) + \left(P_{BES,3}/\eta_{BES,3}\right)} \tag{7}$$

where $P_{BES,1}, P_{BES,2}, P_{BES,3}$ are the BES powers, and $\eta_{BES,1}, \eta_{BES,2}, \eta_{BES,3}$ are the batteries efficiencies for the BES 1, 2 and 3, respectively, and which are defined by Eq. (8).

$$\eta_{BES,i} = \begin{cases} 0.5 * \left(1 + \sqrt{\dfrac{1 - 4 * R_{BES,i} * P_{BES,i}}{\left(V_{BES,i}\right)^2}}\right) discharge \\ 2. \Big/ \left(1 + \sqrt{\dfrac{1 - 4 * R_{BES,i} * P_{BES,i}}{\left(V_{BES,i}\right)^2}}\right) charge \end{cases} \tag{8}$$

where $R_{BES,i}$ and $V_{BES,i}$ are the BES resistance and voltage.

- Power balance:

A linear equality constraint based on the power balance is considered in the EMS to share energy among the BES. According to the BES nominal power and BES output power, the power equality constraint limits the output of the algorithm. The total BESs power ($P_{BES,tot}$) is defined equal to the reference value of each battery obtained from the PI controller.

$$P_{BES,tot} = \sum_{i=1}^{3} P_{BES,i} \tag{9}$$

Since there are three qZSI in series and each one integrates a BES, the equality constrain is applied as

$$A_{eq} \bullet [P_{BES}] = b_{eq} \tag{10}$$

where $A_{eq} = [1\ 1\ 1]$, and $b_{eq} = P_{grid}^* - P_{grid}$.

- Power limits:

The interval that a BES can be charged is set as [$-P_{BES,i}^{max,char}$ 0], and can be discharged in a bounds as [0, $P_{BES,i}^{max,dischar}$]. These two maximum terms of charging and discharging powers are calculated as:

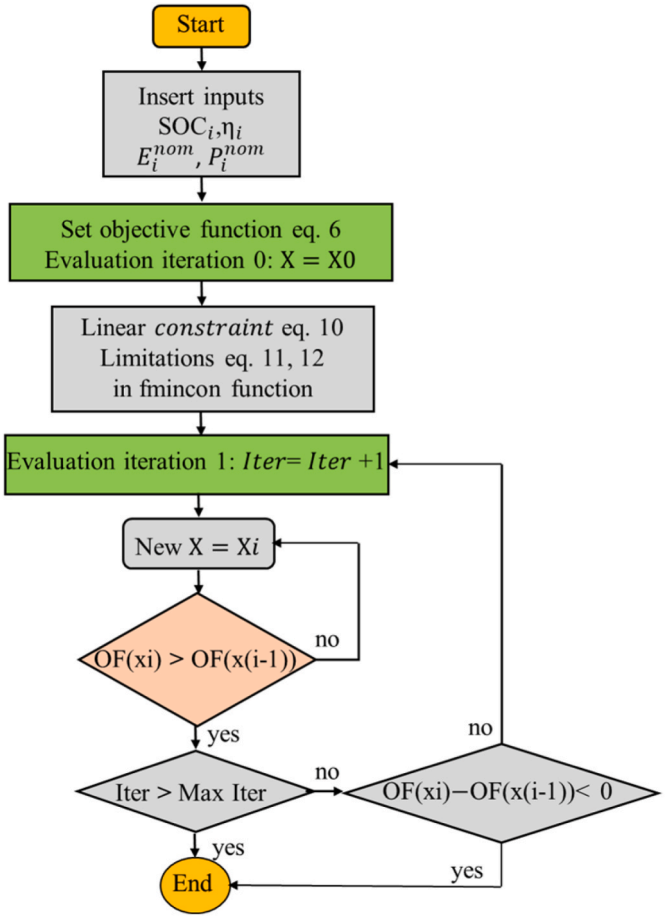

Fig. 6. Optimization flowchart of OPT-EMS.

Table 1
BES parameters.

Param / Battery	Enom (Wh)	Vnom (V)	R (Ω)	Pnom (W)	SOC (%)	Capacity (Ah)
BES1	1200	27.5	0.1261	1200	30	43.63
BES2	1571	30	0.1146	1571	50	52.37
BES3	1986	35	0.1234	1900	85	56.73

$$P_{BES,i}^{max,char} = min\left(P_{BES,i}^{nom}, \frac{E_{BES,i}^{nom}}{\Delta t}.\left(\frac{100 - SOC_{BES,i}}{100}\right)\right) \tag{11}$$

$$P_{BES,i}^{max,dischar} = min\left(P_{BES,i}^{nom}, \frac{E_{BES,i}^{nom}}{\Delta t}.\left(\frac{SOCmin_{BES,i} - SOC_{BES,i}}{100}\right)\right) \tag{12}$$

where $SOCmin_{BES,i}$ is the SOC minimum value of the ith BES that can have, which is chosen based on the manufacturer's recommendations to prevent deep discharging and extend its lifespan; and $E_{BES,i}^{nom}$ is the rated energy of the ith BES.

A minimum term is incorporated into these equations to prevent the BESs from being charged or discharged beyond the values recommended by the manufacturer. This is necessary because during transients, the system may demand unrealistic discharging levels from the BESs or provides unrealistic charging levels. In these equations, a proportional term of BES SOC value to the maximum charging/discharging value is multiplied to the BES nominal energy, which is available over time.

Fig. 6 shows the optimization flowchart and the iterative process employed in this work to converge upon the optimal solution.

The nominal energy and minimum SOC of each BES are considered in the optimal EMS as constraints to avoid issues in the BESs that can reduce their lifetime.

In general, as the number of cascaded modules (integrating RES and BES) increases, the optimal algorithm can be achieved as follows. The total BES efficiency for n BESs can be calculated using the following equation.

$$\eta_{BES} = \frac{P_{BES,1} + P_{BES,2} + P_{BES,3} + \ldots + P_{BES,n}}{P_{BES,1}^{in} + P_{BES,2}^{in} + P_{BES,3}^{in} \ldots + P_{BES,n}^{in}} = \frac{\sum_{i=1}^{n} P_{BES,i}}{\sum_{i=1}^{n} P_{BES,i}^{in}} \tag{13}$$

The power balance (Eq. (9)) is attained by $P_{BES,tot} = \sum_{i=1}^{n} P_{BES,i}$, and the equality constrain (Eq. (10)) by using $A_{eq} = [1\ 1\ 1 \ldots 1]_{1xn}$, and the same b_{eq} to satisfy the power demand.

Additionally, Eqs. (11) and (12) are extended to apply to all modules and limit BESs powers. Finally, the step multilevel voltage waveform is obtained by applying a phase shift of π/n to the adjacent cascaded modules.

While fmincon is a powerful optimization tool, it has its limitations and may not be suitable for all optimization problems. Achieving optimal performance often requires tuning algorithmic options based on problem-specific characteristics, which may not be straightforward. Further, fmincon relies on gradient information (partial derivatives) of the objective function, and if the gradient is difficult or expensive to compute, or if it does not exist, fmincon may not perform well. Additionally, being a local search algorithm, fmincon may converge to a local minimum instead of the global minimum, making it crucial to carefully select the algorithm type, options, tolerance settings and initial guesses. Another limitation of fmincon is its sensitivity to the specification of constraints, especially for problems with poorly conditioned or ill-defined constraints. Therefore, it is essential to carefully design Eqs. (10)–(12) to ensure problem solvability. The most significant challenge in using fmincon for large-scale optimization problems is the computational expense of computing gradients and other required information. Large-scale optimization problems can also require significant memory, making fmincon impractical for problems with a large number of variables. This can hinder the efficiency of fmincon for problems with a large number of decision variables. Despite these limitations, fmincon remains a valuable tool for many optimization problems, particularly when the problem has a well-defined mathematical structure, and the gradient information is readily available, as in the case of the optimization problem addressed in this work.

4. Results and discussion

The results used to evaluate the proposed EMS, denoted as OPT-EMS, with variable RES production components (wind speed and sun irradiation) and reactive-active reference powers requested by the grid operator are presented and discussed in this section. These results are compared with those obtained from a conventional EMS based on the BES SOC and balancing power algorithm, denoted as SOC-EMS, which was used in Ref. [22], and a model predictive control (MPC) EMS similar to that used in Ref. [23].

The SOC-EMS uses a proportional relationship to distribute the total BESs power ($P_{BES,tot}$) among the BES in the discharging mode ($P_{BES,i}^{dischar}$) and in the charging mode ($P_{BES,i}^{char}$) according to their SOC (SOC_i) and depth-of-discharge ($DOD_i = 1 - SOC_i$), respectively:

$$P_{BES,i}^{dischar} = \frac{P_{BES,tot} \bullet SOC_i}{\sum SOC_i} \tag{14}$$

$$P_{BES,i}^{char} = \frac{P_{BES,tot} \bullet DOD_i}{\sum DOD_i} \tag{15}$$

The MPC-EMS controls the battery currents references according to their SOC (SOC_i) and the summation of the BESs power ($P_{BES,\ tot}$). These

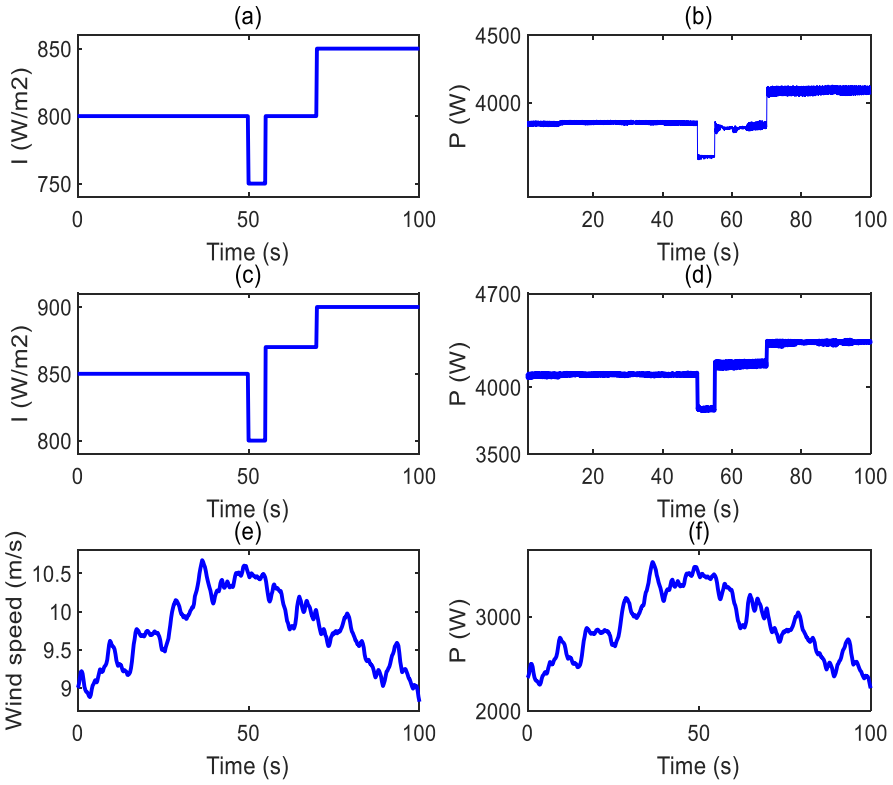

Fig. 7. (a) Irradiance PV1, (b) power PV1, (c) irradiance PV2, (d) power PV2, (e) wind pattern, (f) WT output power.

Table 2
Grid reactive and active power profiles.

Time (s)	P (pu)	Q (pu)
0	2.28	0
10	2.46	0
15	2.46	−0.1
20	2.5	−0.1
30	2.55	−0.3
40	2.5	0
50	2.2	0
55	1.825	0
60	1.75	0
70	1.75	0
75	1.75	0.1
80	1.7	0.1
90	1.65	0.1

Table 3
Simulation setup parameters.

Param	Value	Unit
P_{pv1}	4800	W
P_{pv2}	4800	W
P_{WT}	5000	W
V_{base}	220 $\sqrt{2}$	V
I_{base}	15.42	I
S_{base}	4800	W
D_{nom}	0.2	–
f_{nom}	50	Hz
R_f	0.001	Ohm
L_f	0.005	H
Ts	10^{-6}	S
$V_{nom\text{-}dc}$	159.7	V
$Kp_{\text{-battery-current}}$	0.035	–
$Ki_{\text{-battery-current}}$	2.5	–

control variables are included in a single cost function to be minimized by the MPC. In this regard, quadratic programming (QP) is used as the optimizer solver. Here, the matrices including multiple-input multiple-output (MIMO) system for input (y) and output (u) are:

$$y=\begin{bmatrix} SOC_1 \\ SOC_2 \\ SOC_3 \\ P_{BES,tot} \end{bmatrix} \quad u=\begin{bmatrix} I^{ref}_{BES,1} \\ I^{ref}_{BES,2} \\ I^{ref}_{BES,3} \end{bmatrix} \quad w=\begin{bmatrix} SOC^{ref}_1 \\ SOC^{ref}_2 \\ SOC^{ref}_3 \\ P^{ref}_{BES,tot} \end{bmatrix} \quad \lambda_1=\begin{bmatrix} \tau_1 & 0 & 0 & 0 \\ 0 & \tau_2 & 0 & 0 \\ 0 & 0 & \tau_3 & 0 \\ 0 & 0 & 0 & \tau_4 \end{bmatrix} \quad \lambda_2=\begin{bmatrix} \gamma_1 & 0 & 0 \\ 0 & \gamma_2 & 0 \\ 0 & 0 & \gamma_3 \end{bmatrix} \tag{16}$$

where λ_1, λ_2 are weighting matrices with τ and γ factors.

The cost function optimization is processed through a prediction horizon (P_H). The MPC minimizes the cost function L, which is expressed by:

$$L=\sum_{i=1}^{P_H}[y(k+i|k)-\omega(k+i|k)]^2\lambda_1+\sum_{i=1}^{N}[\Delta u(k+i-1|k)]^2\lambda_2 \tag{17}$$

The deviation of the measured outputs (y) from their reference values (ω) is penalized through L, and the control effort (Δu) tracks the reference signal throughout each time step (k), for every future instant (i), within a prediction horizon (P_H) and a control horizon (N).

The hybrid power plant under study is composed of a 5-kW WT and two independent 4.8 kW photovoltaic cells, with two modules in series and six in parallel for each plant, whose total rated power is 14.4 kW. The impedance network parameters are: $L_1 = L_2 = 0.56mH$, $R_{L1} = R_{L2} = 0.05\ \Omega, C_1 = C_2 = 11mF$ and the selected carrier frequency is f_c = 3.5 kHz. The MPPT voltage reference (47.9V) for PV power plants and WT is updated every 0.008 s by using the MPPT algorithm. The upper and lower MPPT limits are attained by Vdc-ref-Init × 1.15 and Vdc-ref-Init × 0.85. Taking advantage of the qZSI, a Lithium-Ion BES is paralleled with the capacitor $C_{2,i}$ of each qZSI. Three nonidentical BES are considered here that are working under different initial conditions.

Table 1 provides the BES 1, 2 and 3 parameters needed in objective

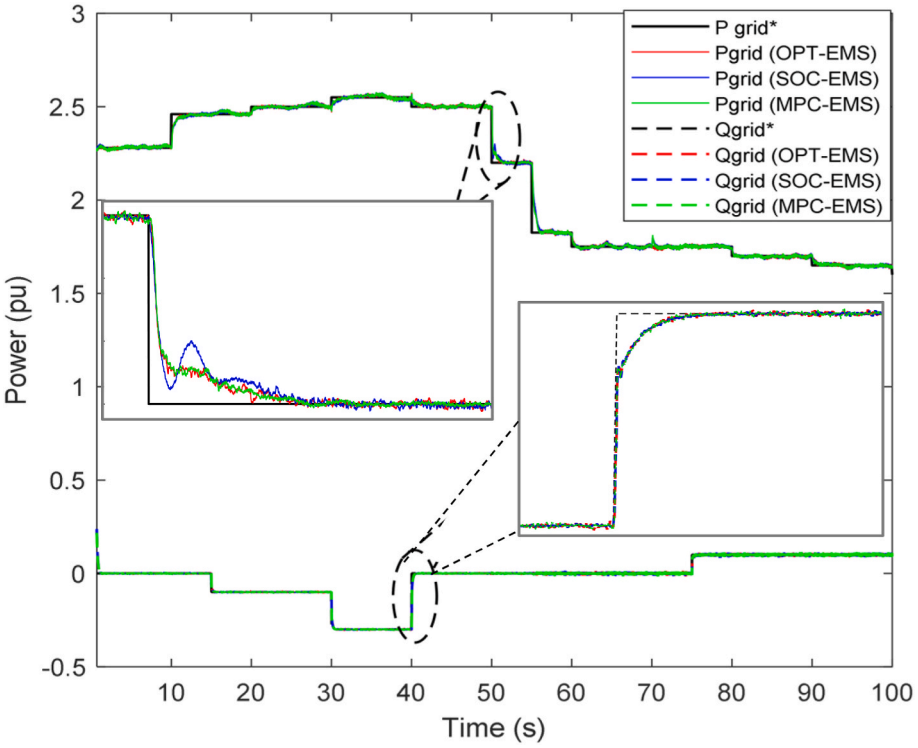

Fig. 8. Reactive and active grid power for OPT-EMS, SOC-EMS, and MPC-EMS.

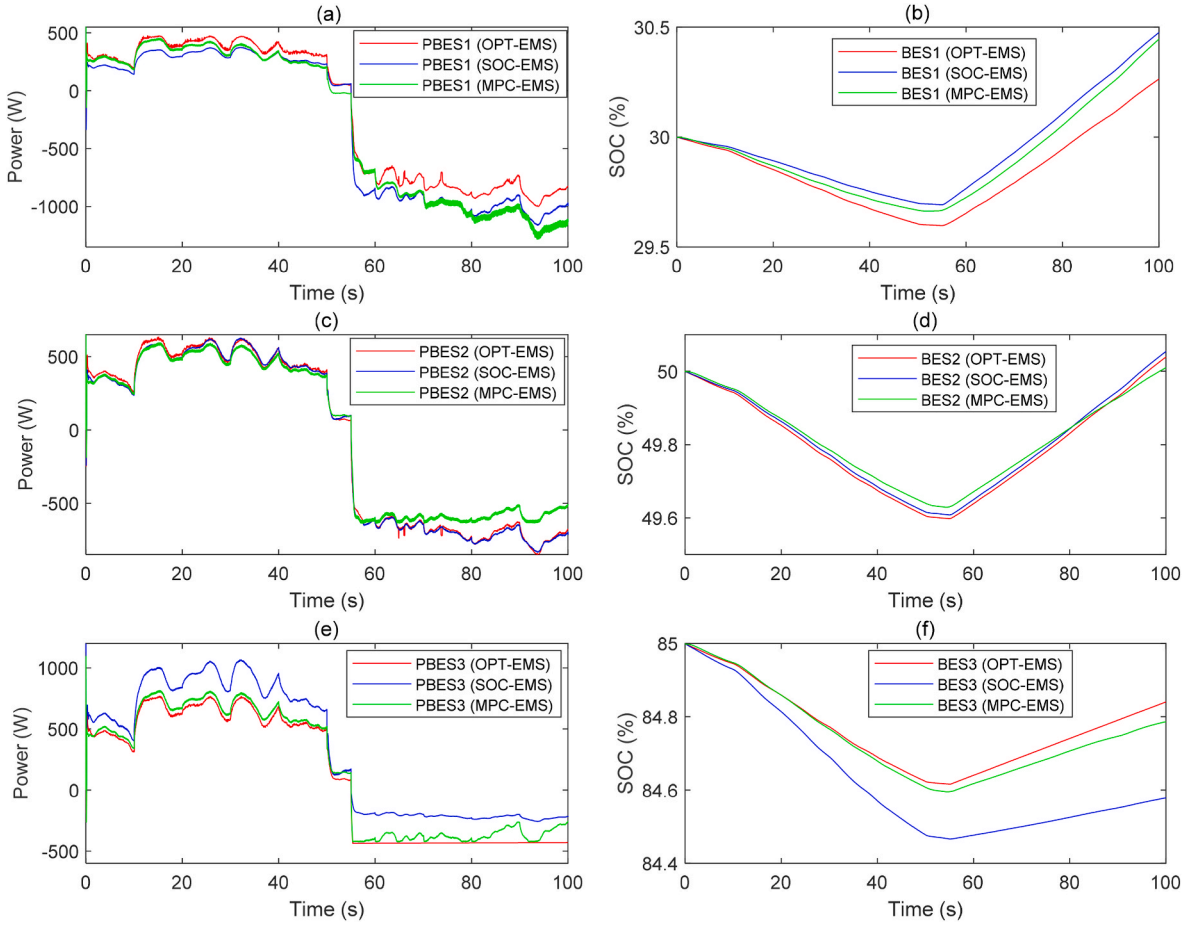

Fig. 9. BES power and SOC value for the three EMSs: (a) BES1 power, (b) SOC1, (c) BES2 power, (d) SOC2, (e) BES3 power, (f) SOC3.

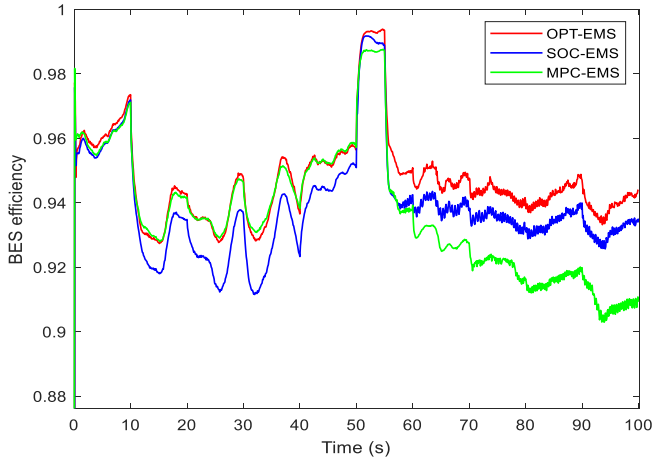

Fig. 10. BES efficiency.

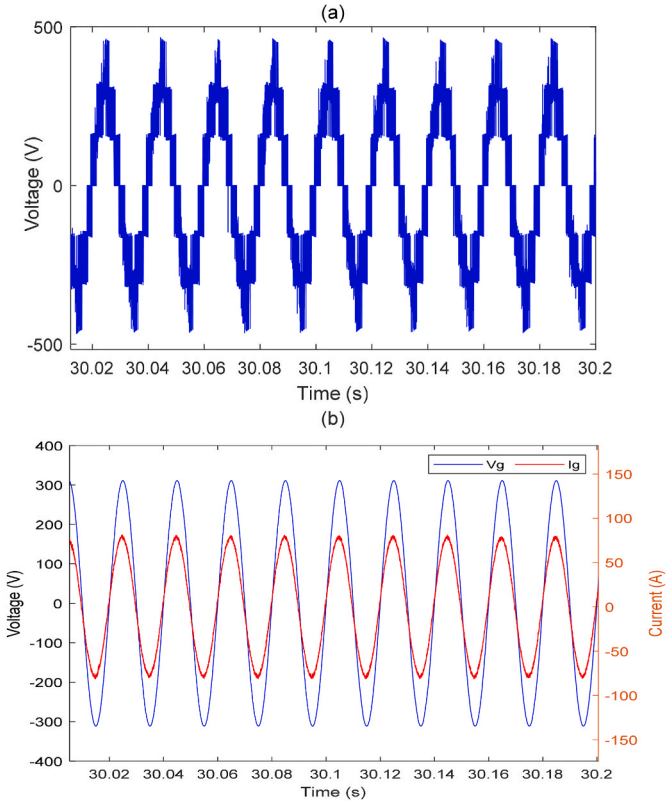

Fig. 11. (a) Inverter output voltage, and (b) Grid components.

Table 4
EMS comparison.

Parameter	SOC-EMS	MPC-EMS	OPT-EMS
Mean value of η_{BES}	0.9380	0.9366	0.9464
Mean value of $P_{BES,i}^{max.dischar}$ (W)	807.26	640.22	594.23
Mean value of $P_{BES,i}^{max.char}$ (W)	−861.52	−980.98	−720.71
$ITAE(P)$	40.38	40.37	40.40
$ITAE(Q)$	12.84	12.84	12.85

function. The BESs can operate between a maximum SOC of 90% and a minimum SOC of 20% to avoid issues in BESs that can reduce their lifetime, which are considered in the implemented EMS.

Fig. 7 illustrates the operating conditions of the RES of the hybrid system: solar radiation and output power of each PV power plant (PV1 and PV2), and the wind speed and WT output power. PV power plants are considered to work under different irradiances conditions. The PV power plants initial conditions are: (PV1): 800 W/m2; (PV2): 850 W/m2. The operating conditions for PV1 changes at t = 50, 55, 70 s to 750, 800, 850 W/m2 and those for PV2 changes at t = 50, 55, 70 s to 800, 870, 900 W/m2. The temperature is kept at 25 °C for both PV plants. A real wind pattern is used for WT with wind speeds between 9 and 11 m/s.

Table 2 presents the grid active and reactive power reference profiles used to assess the operation of the control systems during the simulation. The grid active power references are increased during the first 40 s and decreased after that to evaluate the hybrid power plant in the charging and discharging modes of the BES.

In addition, positive and negative references of grid reactive power are considered to evaluate the hybrid power plant under consumption and generation of reactive power. The simulation set-up parameters are presented in Table 3, where the grid base values and grid filter parameters, simulation sample time, PI gains of the battery current control loop, and inverter nominal voltage are listed.

Fig. 8 illustrates the tracking performance of three EMSs for grid reactive and active powers: OPT-EMS, based on optimizing BES efficiency; SOC-EMS, based on BES SOC and balancing power algorithm; and MPC-EMS, based on model predictive control (MPC). As can be observed, three EMSs meet the demanded powers by the grid in a way that reactive and active power references are properly chased despite the intensive reference changes. Moreover, the results demonstrate the ability of the EMS to maintain accurate tracking performance despite variations in wind speed and solar radiation patterns.

Fig. 9 (a), (c) and (e) shows the batteries power for the three proposed EMS, and Fig. 9 (b), (d) and (f) presents the SOC values and the manner of sharing power among batteries with the initial SOC of: BES1 = 30% < BES2 = 50% < BES3 = 85%. From 0 to 50s, the operator requested power is more than the RES generations power, and thus, the batteries are in the discharging state. From 50 to 55s, the RES total power is somehow the same value as the operator requested power, and therefore, the EMSs don't intensively discharge or charge the BESs (one of the BESs are lightly discharged). After the second 55, the production of RESs is higher than the requested power, and thus, the extra energy is saved in the batteries. In all EMS, BES2 (with an intermediate initial SOC) is discharged and charged in practically the same manner, with an intermediate power compared to BES1 and BES3. BES1 (with the lowest initial SOC) is the least discharged and the most charged BES among the three EMS but presents a higher discharge power and a lower charge power in the OPT-EMS. BES3 (with the highest initial SOC) is the most discharged and the least charged BES in all EMSs, but has a higher discharge power and a lower charge power in the SOC-EMS because the distribution among the BES depends on the BES SOC. The maximum values of the BES discharging and charging powers obtained with the OPT-EMS are lower than those obtained with the SOC-EMS and MPC-EMS to increase the global BES efficiency while properly dispatching power among the BES. From 55 s, BES3 is charged with the OPT-EMS according to the power limit defined by Eq. (11), whereas BES3 with the SOC-EMS is charged with lower power because the SOC-EMS prioritizes charging BES1 with the lowest SOC.

Fig. 10 shows the BES efficiency for EMSs, where it can be seen that the maximum efficiency is reached when the BESs power is near zero. This means that the lower the BES power, the greater the efficiency. The results show that the OPT-EMS has a higher efficiency, and higher differences in the BES efficiency between the EMS appear with the highest BES powers, such as in seconds 25 and 33.

The 7-levels inverter output voltage constructed by the three cascade modules is shown in Fig. 11 (a), and current and voltage of the grid are illustrated in Fig. 11. (b).

Table 4 compares the results obtained by the three EMS in terms of

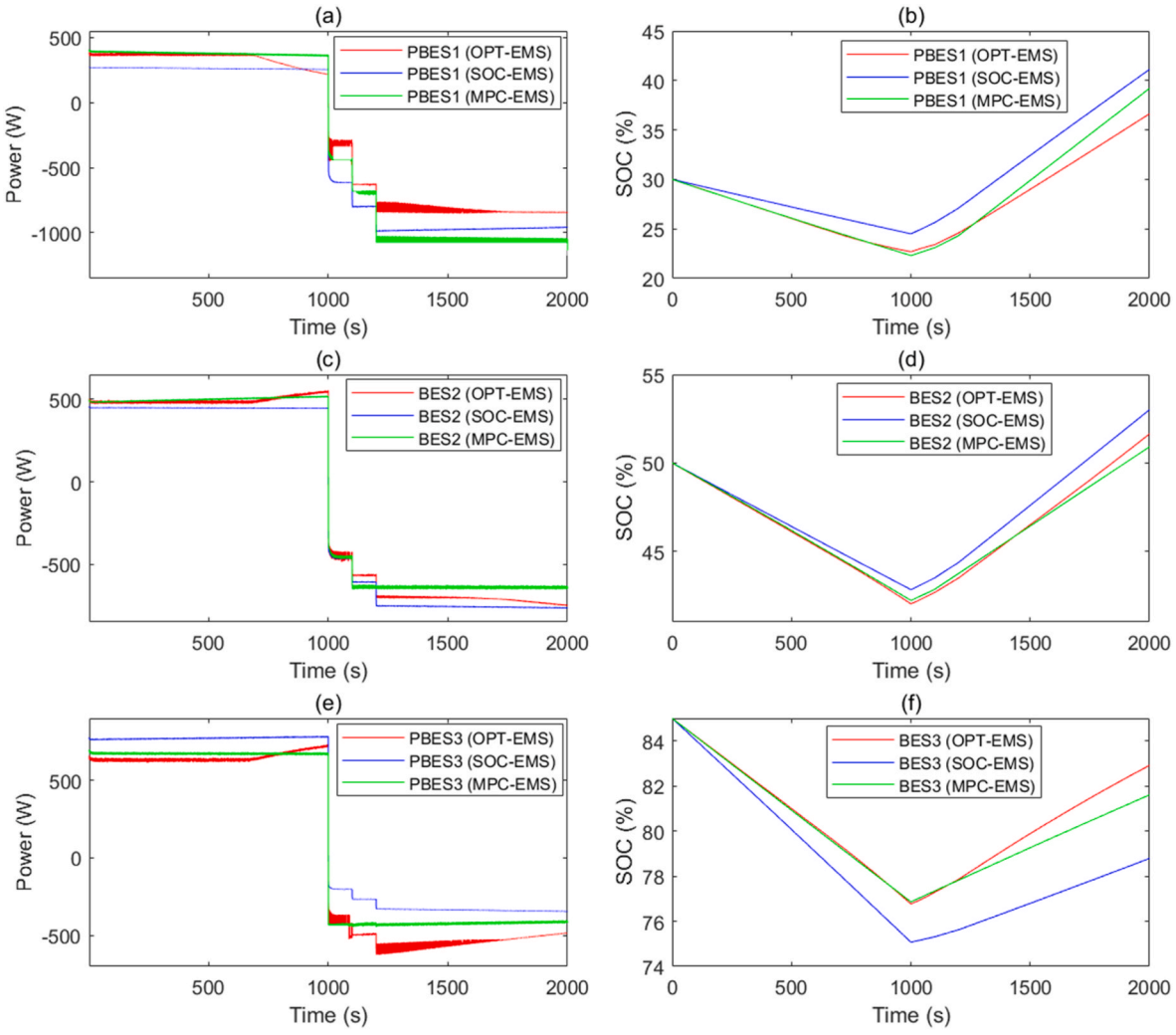

Fig. 12. BES power and SOC value for EMSs: (a) BES1 power, (b) SOC1, (c) BES2 power, (d) SOC2, (e) BES3 power, (f) SOC3.

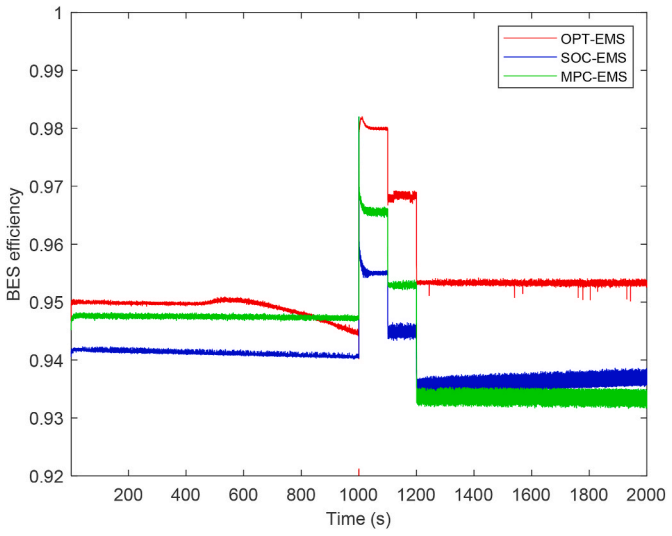

Fig. 13. BES efficiency.

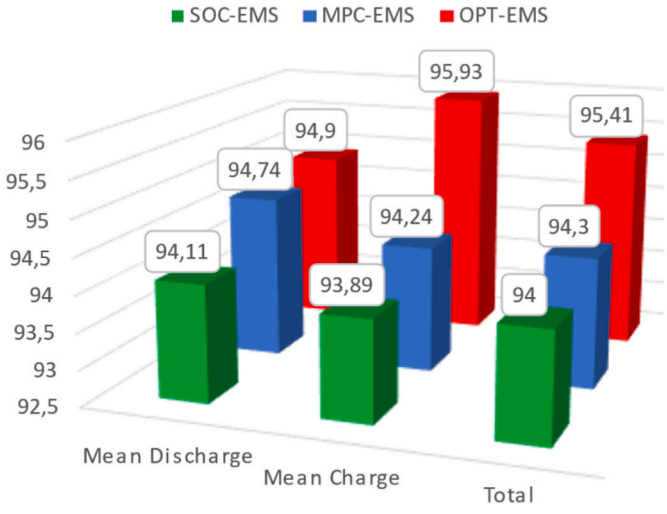

Fig. 14. Comparison of BES efficiency mean values.

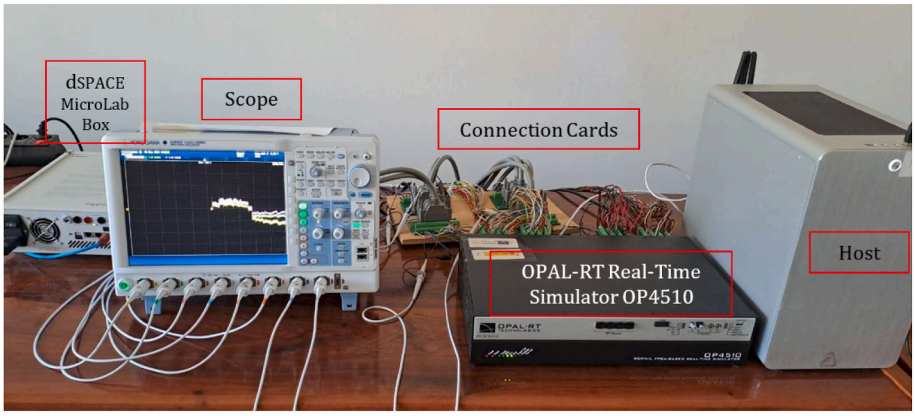

Fig. 15. Experimental setup.

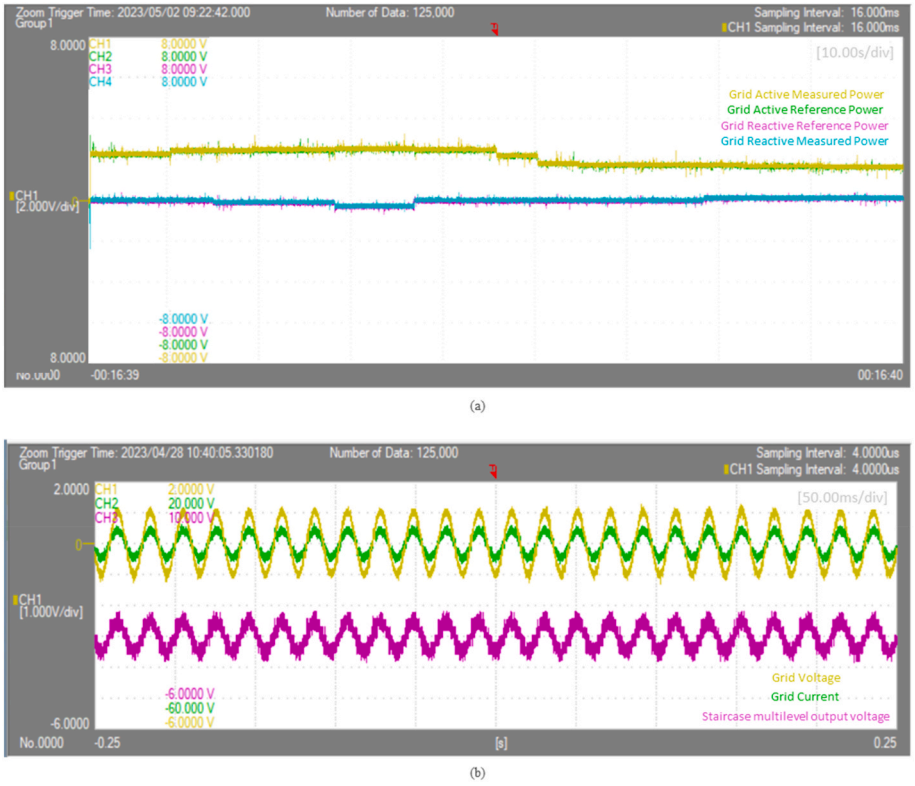

Fig. 16. Experimental results for: (a) OPT-EMS grid reactive and active power, and reference values (b) OPT-EMS grid voltage and current, and 7-level voltage of the BES-qZS-CHBMLI.

global BES efficiency of the hybrid power plant (calculated by Eq. (7)), mean values of $P_{BES,i}^{max,dischar}$ and $P_{BES,i}^{max,char}$, and Integral Time Absolute Error (ITAE) for the grid active (P) and reactive power (Q), which is calculated as follows:

$$ITAE = \int_0^T t|e(t)|dt \tag{18}$$

where $e(t)$ is the gap between the grid active (reactive) power reference and the founded active (reactive) power, and T is the time considered for the study.

The results prove that not only the OPT-EMS tracks properly the grid reactive and active power references, but also significantly increases the global BES efficiency of the hybrid power plant (+0.9% and +1.046% for a 100s simulation) compared to SOC-EMS and MPC-EMS, respectively. The mean values of $P_{BES,i}^{max,dischar}$ and $P_{BES,i}^{max,char}$ achieved with the OPT-EMS are respectively almost 220W and 140W smaller than those with the OPT-EMS and; 46W, 386W for MPC-EMS, and therefore, the proposed OPT-EMS dispatches the power among the BES with smaller power differences among them, instead of prioritizing the BES with the highest SOC a greater discharge, or higher charge of the BES with the lowest SOC, which in turn decrease global BES efficiency of the hybrid power plant.

To further evaluate the performance of the three EMSs under extended operation, a 2000-s simulation was conducted. Fig. 12a, c and 12e illustrate the BES power outputs generated by each EMS, while Fig. 12b, d and 12f depict the corresponding SOC levels. Similar to previous simulations, the OPT-EMS consistently exhibits lower peak discharging and charging power values compared to the SOC-EMS and MPC-EMS. This is attributed to the ability of OPT-EMS to optimize

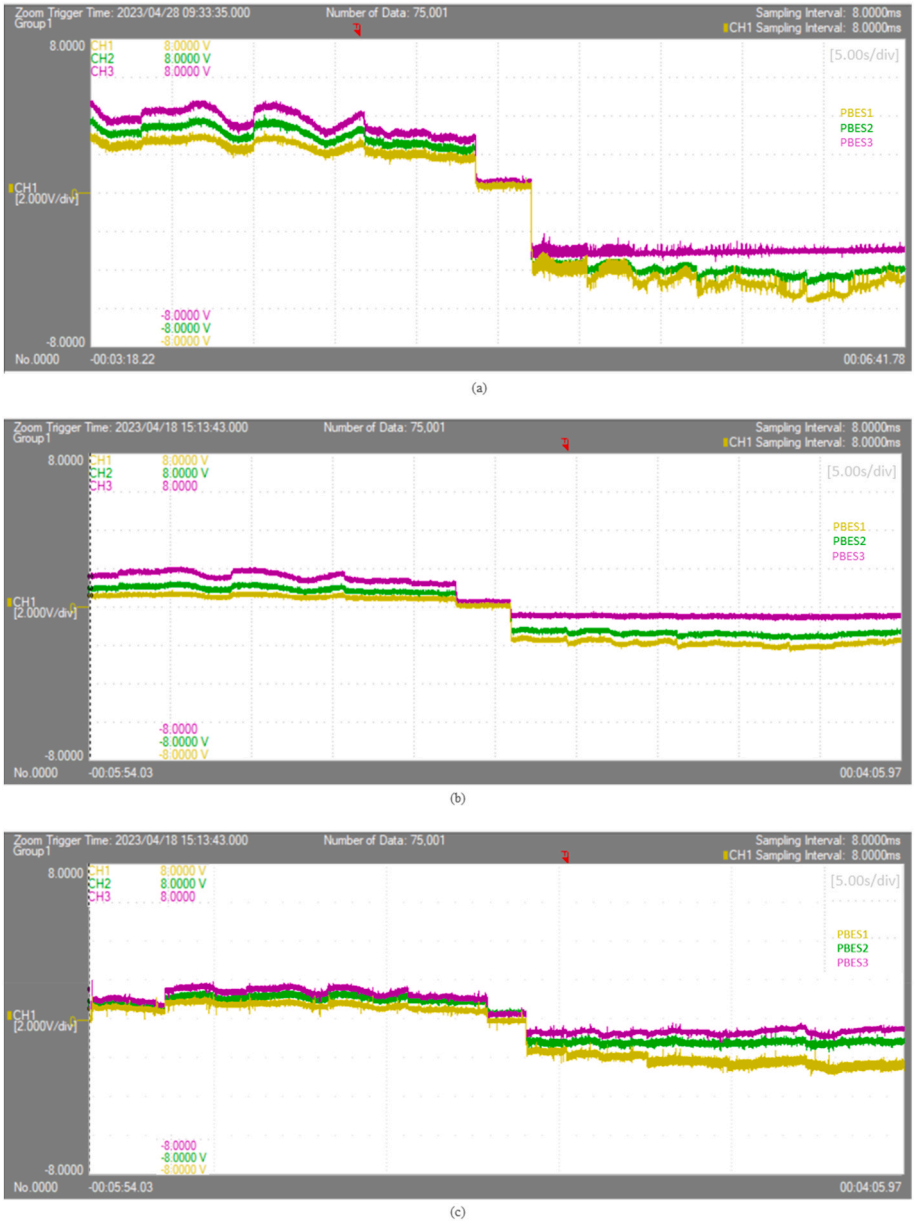

Fig. 17. Experimental results for BES power: (a) OPT-EMS, (b) SOC-EMS, and (c) MPC-EMS.

global BES efficiency while effectively distributing power among the BES units.

From 0 to 1000 s, the BESs are discharged according to the power limits specified in Eq. (12). During this interval, BES3, with the highest SOC, is discharged the most for all EMSs. In particular, the SOC-EMS discharges BES3 to a greater extent than the other BESs, resulting in its lowest efficiency value up to 1000 s, as evident in Fig. 13.

Following 1000 s, the BESs transition into charging mode and are charged according to the power limits defined in Eq. (11). During this period, BES1, with the lowest SOC, is charged the most for all EMSs. Notably, the MPC-EMS charges BES1 more intensively than the other BESs, contributing to its lowest efficiency value after 1000 s, as seen in Fig. 13 during the second half of the simulation.

A graphical comparison of the efficiency mean values of the three EMSs is presented in Fig. 14. For both charging and discharging modes, the OPT-EMS consistently demonstrates superior efficiency, as it leverages an optimizing algorithm to effectively manage BES operations. MPC-EMS also outperforms SOC-EMS overall, but for high charging demand scenarios, SOC-EMS exhibits a slight efficiency advantage.

The experimental tests conducted to prove the effectiveness of the proposed EMS are presented below. These results were collected from an OP4510 real-time OPAL simulator, and the RT-LAB tool was used to monitor and program the model. Through analogue input/output ports, external hardware devices were integrated with the simulator. Moreover, the optimal EMS was implemented in a dSPACE MicroLabBox prototyping unit that allows real-time monitoring, evaluation, and control. Finally, the signals of interest were transferred to a digital storage oscilloscope (DSO) to observe the results obtained from the digital simulator at the analogue output ports. The total hardware connection is schemed in Fig. 15 and a 100 kHz sampling frequency is chosen for the real-time implementation. The representative signals, real-time BESs power, inverter output voltage, and grid voltage-current, are observed through the DSO.

The primary focus of this part lies in evaluating the proposed OPT-EMS under real results, running in real-time on a real control board (MicroLabBox). Fig. 16(a) shows the experimental results for the grid parameters, active and reactive power. Despite significant reference changes, the EMSs demonstrate their ability to effectively track reactive

and active power references. This implies that the EMSs can adapt dynamically and respond to changes in the grid power requirements. Fig. 16(b) shows voltage, current, and the inverter output voltage. The multi-level inverter provides the stepped waveform that closely resembles a sinusoidal waveform by utilizing multiple voltage levels. The simulation results shown in Figs. 8, 11(a) and 11(b) are consistent with these results. The obtained powers of each BES by the OPT-EMS, SOC-EMS, and MPC-EMS are shown in Fig. 17(a) and (b), and 17(c), respectively. For all 3 EMS, during discharging mode, the BES 3 is discharged higher than BES 1,2 due to specific characteristics and settings within the EMSs that prioritize discharging from BES 3 over the others. Similarly, in charging mode, BES 1 is observed to receive the majority of charging power due to its low SOC. Since BES 1 has a lower SOC, the EMSs prioritize charging it more to replenish its energy levels and to bring it to a desired or optimal energy level. It is important to note that the effectiveness of each EMS in managing the ESSs depends on factors such as system specifications, control algorithms, and the specific objectives of the EMS. OPT-EMS is specifically designed to enhance the overall efficiency of the BES system. This suggests that as the individual discharging and charging powers are reduced, the overall efficiency of the BES system improves.

5. Conclusions

This work presented and evaluated, through simulations and experimentally, an EMS based on a constrained nonlinear multivariable algorithm (OPT-EMS) for optimizing the performance of a grid-connected hybrid power plant comprising WT, PV power plants, and different BESs integrated into a BES-qZS-CHBMLI configuration.

The proposed EMS prioritizes both BES efficiency and lifespan while ensuring the overall system power balance. This OPT-EMS was compared with two EMSs (SOC-EMS and MPC-EMS) under varying renewable energy resources and grid active and reactive power requirements. The three EMSs were implemented on a real control card, MicroLabBox, and tested in real time in a HIL system based on OPAL-RT, demonstrating the applicability of the new EMS developed in this paper.

The results revealed that the OPT-EMS achieved comparable grid power tracking performance to the SOC-EMS and MPC-EMS, while efficiently distributing excess/deficit power among the BESs, leading to a higher global BES efficiency of the hybrid power plant: +0.84% (+1.41%) over the SOC-EMS and +0.98% (1.11%) over the MPC-EMS for a 100-s (2000-s) simulation.

For future work, it could be studied the incorporation of new ESSs in the hybrid power plant, such as hydrogen systems (fuel cell and electrolyzer), new optimization problems, such as the optimization of operating costs of the components of the hybrid power plant, or the application of stochastic optimization algorithms, such as evolutionary algorithms, could be used for addressing the global optimization challenges associated with the proposed complex objective functions.

CRediT authorship contribution statement

Ehsan Hosseini: Conceptualization, Formal analysis, Investigation, Methodology, Writing – original draft. **Pablo Horrillo-Quintero:** Conceptualization, Formal analysis, Investigation, Methodology, Writing – original draft. **David Carrasco-Gonzalez:** Investigation, Methodology, Writing – original draft. **Pablo García-Triviño:** Formal analysis, Investigation, Methodology, Writing – original draft. **Raúl Sarrias-Mena:** Formal analysis, Investigation, Methodology, Writing – original draft. **Carlos A. García-Vázquez:** Formal analysis, Methodology, Writing – original draft. **Luis M. Fernández-Ramírez:** Conceptualization, Funding acquisition, Methodology, Project administration, Supervision, Writing – review & editing.

Declaration of competing interest

The authors declare that they have no known competing financial interests or personal relationships that could have appeared to influence the work reported in this paper.

Data availability

Data will be made available on request.

Acknowledgments

This work was partially supported by the Regional Ministry of Economic Transformation, Industry, Knowledge, and Universities of Junta de Andalucía (under Grant PY20_00317), and Ministerio de Ciencia e Innovación, Agencia Estatal de Investigación, FEDER, UE (Grant PID2021-123633OB-C32 supported by MCIN/AEI/10.13039/501100011033/FEDER, UE).

References

[1] Sousa J, et al. Renewable energy communities optimal design supported by an optimization model for investment in PV/wind capacity and renewable electricity sharing. Energy Nov. 2023;283:1–14. https://doi.org/10.1016/j.energy.2023.128464.
[2] Auguadra M, Ribó-Pérez D, Gómez-Navarro T. Planning the deployment of energy storage systems to integrate high shares of renewables: the Spain case study. Energy Feb. 2023;264:1–17. https://doi.org/10.1016/j.energy.2022.126275.
[3] Oliveira-Assis L, et al. Simplified model of battery energy-stored quasi-Z-source inverter-based photovoltaic power plant with Twofold energy management system. Energy Apr. 2022;244:1–11. https://doi.org/10.1016/j.energy.2021.122563.
[4] Chen Y, Li R, Sun Z, et al. SOC estimation of retired lithium-ion batteries for electric vehicle with improved particle filter by H-infinity filter. Energy Rep Dec. 2023;9(3):1937–47. https://doi.org/10.1016/j.egyr.2023.01.018. 2021.
[5] Roccaforte F, Giannazzo F, Greco G. Ion Implantation doping in silicon carbide and gallium nitride electronic devices. Micro Jan. 2022;2(1):23–53. https://doi.org/10.3390/MICRO2010002.
[6] Q. Tana, L. Mao, Y. Cai, B. Zhang, Z. Ruan, "Comparative evaluation and analysis of GaN-based VSIs and CSIs," Energy Rep, Vol. 9, pp.568-576. doi: https://doi.org/10.1016/j.egyr.2022.11.082.
[7] Zhang G, et al. An extendable single-switch n-cell boost converter with high voltage gain and low components stress for renewable energy. Int J Circ Theor Appl Jun. 2020;48(6):817–31. https://doi.org/10.1002/cta.2801.
[8] Wu B, Narimani M. High-power converters and AC Drives": eBook. second ed. Wiley; 2016. https://doi.org/10.1002/9781119156079.
[9] Taul MG, Pallo N, Stillwell A, Pilawa-Podgurski RCN. Theoretical analysis and experimental validation of flying-capacitor multilevel converters under short-circuit fault conditions. IEEE Trans Power Electron 2021;36(11). https://doi.org/10.1109/TPEL.2021.3075447.
[10] Sharna V. Diode clamped multilevel inverter switching topology. International Journal of Industrial Electronics and Electrical Engineering 2017;5.
[11] Y. Liu, "Impedance source power electronic converters", eBook, Wiley, pp. 1-424, Accessed: February. 15, 2023. [Online]. Available: https://www.wiley.com/enes/Impedance+Source+Power+Electronic+Converters-p-9781119037071.
[12] Ellabban O, Abu-Rub H, Source Inverter Z. Topology improvements review: Z-source inverter,". IEEE Industrial Electronics Magazine Mar. 2016;10(1):6–24. https://doi.org/10.1109/MIE.2015.2475475.
[13] Sun D, Ge B, Peng FZ, Haitham AR, Bi D, Liu Y. A new grid-connected PV system based on cascaded H-bridge quasi-Z source inverter. IEEE International Symposium on Industrial Electronics May.2012. https://doi.org/10.1109/ISIE.2012.6237218.
[14] Kadwane SG, Kadu A, Fulzele Research P, Alviya Mahevashand D. Control strategy for closed control of quasi-Z source based cascaded H-bridge inverter. In: 2021 innovations in power and advanced computing technologies (i-PACT); 2021. https://doi.org/10.1109/IPACT52855.2021.9696736. Control Strategy for Closed Control of Quasi-Z Source Based Cascaded H-bridge Inverter.
[15] Manoj P, Annamalai K, Member S, Dhara S, Student Member G, Somasekhar VT. A quasi-Z-source-based space-vector-modulated cascaded four-level inverter for photovoltaic applications. IEEE J Emerg Sel Top Power Electron 2022;10(4):4749. https://doi.org/10.1109/JESTPE.2021.3125695.
[16] Zhou Y, Member S, Liu L, Member S, Li H. A high-performance photovoltaic module-integrated converter (MIC) based on cascaded quasi-Z-source inverters (qZSI) using eGaN FETs. IEEE Trans Power Electron 2013;28(6). https://doi.org/10.1109/TPEL.2012.2219556.
[17] Chettibi N, Mellit A. Intelligent control strategy for a grid connected PV/SOFC/BESS energy generation system. Energy Feb. 2018;147:239–62. https://doi.org/10.1016/j.energy.2018.01.030.
[18] Tahani M, Babayan N, Pouyaei A. Optimization of PV/Wind/Battery stand-alone system, using hybrid FPA/SA algorithm and CFD simulation, case study: Tehran. Energy Convers Manag 2015;106:644–59.

[19] Liang W, Liu Y, Peng J. A Day and night operational quasi-Z source multilevel grid-Tied PV power system to achieve active and reactive power control. IEEE Trans Power Electron 2021;36(1). https://doi.org/10.1109/TPEL.2020.3000818.
[20] Liang W, Liu Y, Abu-Rub H. State-of-charge balancing control for battery energy stored quasi-Z source cascaded multilevel inverter based photovoltaic power system. In: 2015 IEEE energy conversion congress and Exposition (ECCE); 2015. https://doi.org/10.1109/ECCE.2015.7309662.
[21] Ge B, Liu Y, Abu-Rub H, Peng FZ. State-of-Charge balancing control for a battery-energy-stored quasi-Z-source cascaded-multilevel-inverter-based photovoltaic power system. IEEE Trans Ind Electron 2018;65(3). https://doi.org/10.1109/TIE.2017.2745406.
[22] Horrillo-Quintero P, García-Triviño P, Sarrias-Mena R, Andrés García-Vázquez C, Fernández-Ramírez LM. Control system for quasi-Z-source cascaded H-bridge multilevel inverter with PV power generation and battery energy storage system. In: Interdisciplinary conference on mechanics, computers and electrics (ICMECE 2022); 2022. Barcelona, Spain.
[23] Lashab A, Sera D, Guerrero JM. Model predictive control of cascaded multilevel battery assisted quasi Z-source PV inverter with reduced computational effort. IEEE Energy Conversion Congress and Exposition (ECCE) Nov. 2019. https://doi.org/10.1109/ECCE.2019.8912551.
[24] Kabalci Ersan. Multilevel inverters: introduction and emergent topologies. first ed. eBook, Academic Press; 2021.
[25] Horrillo-Quintero P, García-Triviño P, Sarrias-Mena R, Andrés García-Vázquez C, Fernández-Ramírez LM. Active and reactive power sharing for PV power plants with quasi-Z-source cascaded H-bridge multilevel inverters. In: 4th international conference on smart power & internet energy systems (SPIES 2022); 2022. p. 1956–61.